Shock Wave-Induced Phase Transition in RDX Single Crystals

ARTICLE *in* THE JOURNAL OF PHYSICAL CHEMISTRY B · OCTOBER 2007

Impact Factor: 3.3 · DOI: 10.1021/jp079502q · Source: PubMed

3 AUTHORS, INCLUDING:

Zbigniew Dreger
Washington State University
124 PUBLICATIONS **1,127** CITATIONS

SEE PROFILE

Shock Wave-Induced Phase Transition in RDX Single Crystals

James E. Patterson, Zbigniew A. Dreger,* and Yogendra M. Gupta

Institute for Shock Physics and Department of Physics, Washington State University Pullman, Washington 99164-2816

Received: January 17, 2007

The real-time, molecular-level response of oriented single crystals of hexahydro-1,3,5-trinitro-*s*-triazine (RDX) to shock compression was examined using Raman spectroscopy. Single crystals of [111], [210], or [100] orientation were shocked under stepwise loading to peak stresses from 3.0 to 5.5 GPa. Two types of measurements were performed: (i) high-resolution Raman spectroscopy to probe the material at peak stress and (ii) time-resolved Raman spectroscopy to monitor the evolution of molecular changes as the shock wave reverberated through the material. The frequency shift of the CH stretching modes under shock loading appeared to be similar for all three crystal orientations below 3.5 GPa. Significant spectral changes were observed in crystals shocked above 4.5 GPa. These changes were similar to those observed in static pressure measurements, indicating the occurrence of the $\alpha-\gamma$ phase transition in shocked RDX crystals. No apparent orientation dependence in the molecular response of RDX to shock compression up to 5.5 GPa was observed. The phase transition had an incubation time of ~100 ns when RDX was shocked to 5.5 GPa peak stress. The observation of the $\alpha-\gamma$ phase transition under shock wave loading is briefly discussed in connection with the onset of chemical decomposition in shocked RDX.

I. Introduction

Characteristics of high explosives (HE), such as performance, sensitivity, and stability, are determined by molecular level phenomena. These properties have implications for safety and handling as well as the practical use of HE materials. To predict and tailor the properties of new energetic materials, a good understanding of the material properties at multiple length scales is needed. This study is part of a comprehensive effort to investigate the molecular level response of HE single crystals to shock loading to gain insight into molecular mechanisms governing shock-induced decomposition. Previously, we have reported on the energetic molecular crystal, pentaerythritol tetranitrate (PETN).[1−3]

Continuum measurements have shown that the shock initiation of PETN single crystals is strongly anisotropic.[4,5] Shock compression along the sensitive [110] direction results in hindered shear across a slip plane, whereas no such hindrance occurs for shocks along the insensitive [100] direction. It has been shown, both theoretically[1,3] and experimentally,[3,6] that this hindered shear can lead to conformational changes of individual PETN molecules, resulting in increased sensitivity. Shock compression-induced shifting of the frequencies of certain Raman modes was also shown to have an orientation dependence.[6] Thus, anisotropy has been observed in shocked PETN at both the macroscopic and molecular levels.

To determine whether these findings are specific to PETN or applicable to HE crystals generally, we examined the shock response of oriented single crystals of hexahydro-1,3,5-trinitro-*s*-triazine (RDX). Reported elastic constants of RDX suggest the possibility of anisotropic sensitivity,[7−9] but this has yet to be demonstrated under shock wave loading. Recent wave profile measurements at 2.5 GPa indicate some anisotropy in the continuum response of RDX single crystals.[10] However, these experiments were all performed well below the initiation threshold (10−13 GPa).[11] No molecular-level anisotropy has been reported for shocked RDX. Unlike PETN, plane shock wave studies on RDX single crystals are very limited.[12−15]

RDX is known to exist in three polymorphic phases, termed α, β, and γ.[16−21] Only the structure of the ambient α phase is fully known.[22] The transition between the α and γ phases occurs at ~3.8 GPa and is detectable by changes in the Raman spectrum.[20,23] This phase transition has not been observed previously under shock compression. However, if it occurs, it would represent an important event prior to initiation and would necessitate a thorough investigation of the γ phase structure. The β phase is a high-temperature, high-pressure phase[18,19] and may play a role in the later stages of initiation.

Although decomposition mechanisms for RDX have been proposed, on the basis of experimental[24] and computational[25,26] efforts, the applicability of these mechanisms to shock initiation is unclear. A variety of preliminary investigations have been attempted to examine shocked RDX at the molecular level.[11,12−15] Cleavage of a single N−N bond has been proposed as the initial reaction step, but evidence at present is circumstantial.[12,27] Previous Raman measurements[14,15] involved crystals of unspecified orientations and considered modes that recent static pressure experiments[23] have shown to be relatively insensitive to pressure. Therefore, there is a need for careful Raman measurements in well characterized shock wave experiments on oriented RDX single crystals.

Here, we report on two types of Raman measurements: (i) high-resolution Raman spectroscopy[6] to probe the crystal in the peak state, and (ii) time-resolved Raman spectroscopy[28−30] to examine the time-varying response of RDX to shock compression. Changes in the CH stretching region (2800−3200 cm^{-1}) were monitored because these modes exhibited large orientation dependent shifts in PETN[6] and are a good indicator of the $\alpha-\gamma$ phase transition in RDX.[20,23] Comparisons between Raman

* Corresponding author. E-mail: dreger@wsu.edu.

10.1021/jp079502q CCC: $37.00
Published on Web 08/24/2007

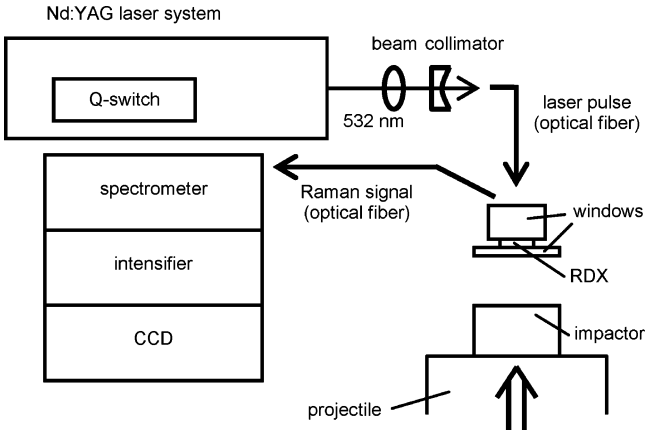

Figure 1. Schematic view of the experimental configuration for high-resolution Raman measurements. A single 532 nm pulse from a Nd:YAG laser is used for Raman excitation. The Raman scattered light is recorded by the spectrometer−intensifier−CCD detection system.

TABLE 1: Raman Frequencies of Selected Modes of RDX at Ambient Conditions

frequency (cm^{-1})			
single crystal[a]	powder[b]	calculated[c]	assignment[c]
3076	3075	3206	CH stretch (eq)
		3205	CH stretch (eq)
3067	3067	3199	HCH stretch
3003	3001	3081	HCH stretch
2949	2949	3016	CH stretch (ax)
		3015	CH stretch (ax)
2906			Combination[d]

[a] Ref 23. [b] Ref 36. [c] Ref 38, except where indicated. [d] Ref 37.

spectra obtained under shock loading and under hydrostatic compression[23] are reported.

As a prelude to understanding the chemical decomposition of shocked RDX, we have focused on the response of RDX below the initiation threshold and in the vicinity of the $\alpha-\gamma$ phase transition (observed under static high-pressure conditions at ~3.8 GPa).[20,21,23] We have attempted to address the following specific questions: (i) does the $\alpha-\gamma$ phase transition occur under shock loading, (ii) does shocked RDX exhibit anisotropy at the molecular level at stresses close to the phase transition, and (iii) is there a time-dependence associated with the phase transition? Investigating the structural response of RDX is an important first step because changes in molecular structure and orientation are expected to be important for shock initiation.

The remainder of this paper is organized as follows. The next section describes the experimental methods. Results and discussion are presented in Section III, and Section IV contains concluding remarks.

II. Experimental Approach and Methods

Shock wave experiments were performed on RDX single crystals grown at the Los Alamos National Laboratory (LANL) from stock produced by the Woolwich (HMX-free) process with subsequent purification before crystallization. The crystals were oriented, cut, and provided to us by Dr. Daniel E. Hooks of LANL. Samples were oriented along one of three crystallographic directions: [111], [210], or [100]. These orientations were chosen on the basis of the available knowledge of the RDX slip systems. Three slip systems have been reported for RDX at ambient pressure: (010) [001], (021) [100], and $(0\bar{2}1)$ [100], the last two being symmetry equivalent.[31] Using the approach of Johnson et al.,[32] shocks propagated along the [111] direction can be shown to activate all three systems, whereas shocks along the [210] direction can activate only the two symmetry equivalent systems. No known slip systems are activated by shocks along the [100] direction.[33]

TABLE 2: Summary of Shock Experiments

no.	experiment type	crystal orientation	sample thickness (μm)	projectile velocity (km/s)	peak stress (GPa)
1	high resolution	[111]	413	0.612	5.47
2	high resolution	[210]	418	0.619	5.54
3	high resolution	[111]	412	0.347	3.01
4	high resolution	[111]	396	0.506	4.47
5	high resolution	[111]	400	0.402	3.51
6	high resolution	[100]	426	0.348	3.02
7	high resolution	[100]	416	0.615	5.50
8	high resolution	[210]	420	0.348	3.02
9	time-resolved	[111]	409	0.621	5.56

Typical lateral dimensions of the samples were 7−8 mm. The crystals were ground to a thickness of ~400 μm and polished to an optical finish with aluminum oxide lapping sheets. The polished RDX crystal was then sandwiched between two Z-cut quartz windows with a thin film of liquid glycerol (spectroscopic grade, Aldrich Chemical) between the crystal and the windows. The front and back windows were 2 mm and 9.5 mm thick, respectively.

Figure 1 shows the configuration of our impact experiments using the high-resolution Raman detection system, which is similar to that used in the PETN work.[6] Planar shock waves were produced by impacting the sample assembly with a Z-cut quartz crystal of 12.7 mm thickness. The impactor crystal was mounted on a projectile launched using a single stage light-gas gun. On impact, a shock wave propagated through the front quartz window and into the RDX crystal. Because of the impedance mismatch between Z-cut quartz and RDX, the sample was compressed under stepwise loading. The final stress state in the RDX is known accurately because it depends only on the shock wave response of elastically compressed Z-cut quartz and the impact velocity. Stress histories in the RDX crystal were calculated using a 1-dimensional wave propagation code[34] and a material model for RDX.[35] Peak stresses were between 3.0 and 5.5 GPa.

Two experimental techniques, developed in our laboratory, were used to obtain the Raman spectra, and details regarding the same can be found in references 6 and 28−30. The spectral range of interest for this study was the CH stretching region from 2800 to 3200 cm^{-1}. A summary of the Raman modes in this range at ambient pressure, including their frequencies and assignments based on experiments[23,36,37] and DFT calculations,[38] is presented in Table 1. Table 2 summarizes the details of our impact experiments.

High-resolution Raman measurements[6] (see Figure 1) were performed by illuminating the sample with a single pulse from a Q-switched frequency doubled Nd:YAG laser (532 nm). Typical laser pulse energies were between 8.5 and 10 mJ with a pulse duration of 20 ns. Back-scattered light was collected using an optical fiber and transported to a 0.5 m spectrometer; a holographic notch filter was used to reject the elastically scattered 532 nm light. The spectrometer output was amplified with a gated image intensifier and then detected using a back-illuminated CCD. The overall spectral resolution of the detection system was ~3.5 cm^{-1}. The intensifier was gated between 80

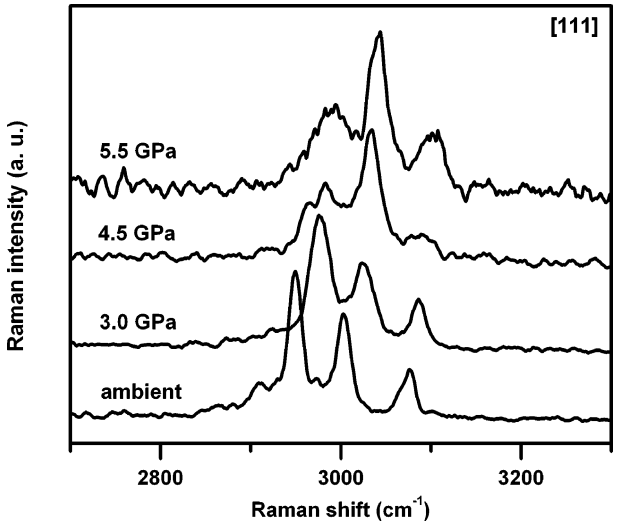

Figure 2. Raman spectra of the C−H stretching modes of RDX single crystals of [111] orientation at ambient conditions and under shock at 3.0, 4.5, and 5.5 GPa peak stress. The relative intensity and shape of the peaks change between 3.0 and 4.5 GPa. Spectra are offset vertically for clarity in this and subsequent figures.

and 120 ns to reject extraneous light due to emission by the RDX crystal or any other source.

For time-resolved measurements,[28−30] a tunable flash lamp-pumped dye laser at 514.5 nm was used as the excitation source. The pulse duration was 2 μs, and pulse energy was 65 mJ. Backscattered light was passed through a holographic notch filter to remove elastically scattered 514.5 nm light and sent to an imaging spectrometer having a holographic grating. The spectrally dispersed light was coupled to a streak camera, followed by an intensified CCD to provide a time-resolved record of spectral changes. Spectra at particular times were generated by binning (averaging) over an appropriate number of tracks on the time axis. The spectral resolution of this system was ~25 cm^{-1}. The time resolution, determined by the spot size on the detector, was ~40 ns.

Raman measurements under static high pressure[23] complemented the shock experiments. In these experiments, a single crystal of RDX of arbitrary orientation was compressed in a diamond anvil cell (DAC) using argon as a hydrostatic pressure medium. Raman spectra were obtained with a polarized Ar ion laser (514.5 nm) as the excitation source. The spectral resolution was ~1 cm^{-1}. The pressure ranged from ambient to 6 GPa in roughly 0.5 GPa steps. Details of the experimental approach for static pressure measurements can be found in references 23 and 39.

III. Results and Discussion

A. Stress Dependence. Selected spectra from the high-resolution Raman measurements on [111]-oriented RDX single crystals are shown in Figure 2. The spectra were smoothed by 10-point adjacent averaging. Between ambient pressure and 3.0 GPa, the Raman modes shift to higher frequency and broaden slightly. The spectrum at 4.5 GPa exhibits a significant change in the spectral shape and relative intensity of the modes. From 4.5 to 5.5 GPa, the Raman modes shift further to higher frequency with the overall shape unchanged.

To better understand the response of RDX to shock compression, it is instructive to compare the Raman spectra obtained under shock loading to static pressure measurements at similar stresses. Despite the different loading states in the two cases (the shock state is one of uniaxial strain, whereas the static pressure state is hydrostatic), such comparisons are valuable because both sets of data are at comparable densities. Figure 3a contains static pressure Raman spectra of RDX single crystals at ambient conditions, 2.95 and 5.5 GPa.[23] Note the multiplication of Raman peaks in the 5.5 GPa spectrum. This splitting has been attributed to Davydov splitting and indicates a structural change accompanying the phase transition.[23]

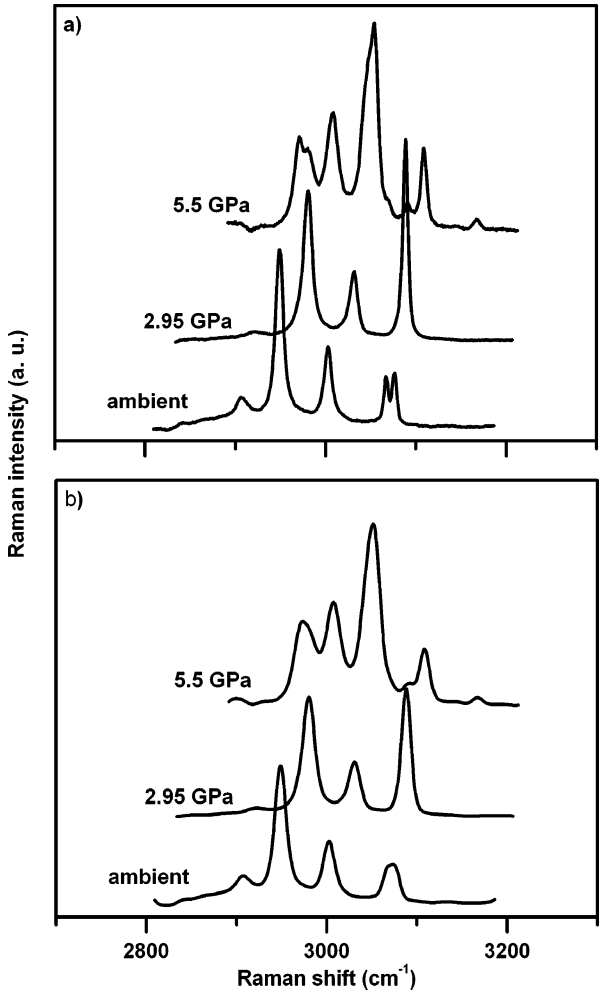

Figure 3. (a) Static pressure Raman spectra of RDX single crystal (arbitrary orientation) at ambient pressure, 2.95, and 5.5 GPa. (b) Static pressure spectra after convolution with a Gaussian response function to give comparable spectral resolution to the high-resolution Raman system.

As indicated earlier, the detection system for the static pressure measurements had a higher spectral resolution than the systems used for the shock experiments. To permit consistent comparisons between the two sets of data, the ambient spectrum obtained with the static high-pressure system was broadened through convolution, using a Gaussian response function, to match the peak width of the 2949 cm^{-1} mode measured by the Raman system used for shock experiments. This function was then applied to the spectra taken at higher static pressures. The broadened spectra, shown in Figure 3b, should be viewed as static pressure spectra that incorporate the instrument broadening typical of our shock wave measurements. Even with the lower spectral resolution, differences between the spectra at 2.95 and 5.5 GPa are clearly seen in Figure 3b. These spectral changes indicate the occurrence of the $\alpha-\gamma$ phase transition under static pressure conditions.[20,23]

Note the good agreement between the ambient spectrum shown in Figure 2 and the ambient spectrum in Figure 3b. There

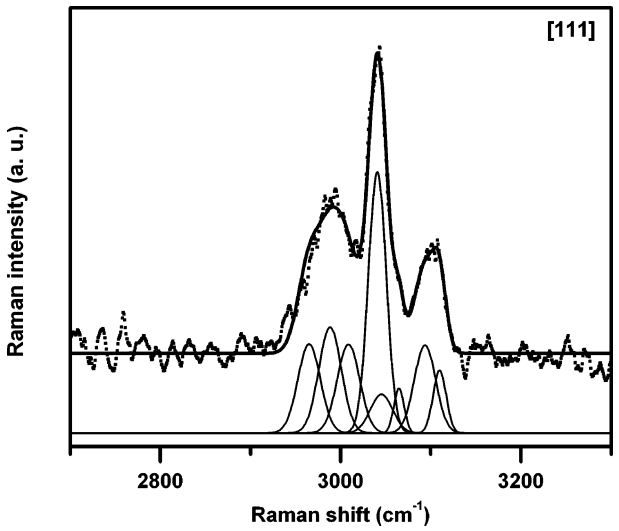

Figure 4. Example of peak-fitting applied to the Raman spectrum of [111]-oriented RDX at 5.5 GPa peak stress. The spectrum is well-fit by eight Gaussian peaks. Peak positions were based on the static pressure spectrum.

is also good agreement between the position of the Raman modes in the static pressure 2.95 GPa spectrum in Figure 3b and the 3.0 GPa shock result in Figure 2. The relative intensities of the peaks are different because changing the crystal orientation relative to the laser beam leads to changes in the relative intensities of the Raman modes; the crystal orientation was arbitrary in the static pressure experiments. At 5.5 GPa, the static and shock results show overall similarity, but not all the details are the same. Figure 3b clearly shows two bands at ~3000 cm^{-1}, whereas the spectrum of shocked RDX in Figure 2 shows a single, broad feature. This difference is likely caused by peak broadening due to shock loading and intensity changes due to orientation. Under shock loading, there is an intense central peak around 3045 cm^{-1} with two broad bands to either side. Each of these broad bands consists of multiple peaks.

Using the static pressure Raman spectra as a guide, the high-resolution Raman spectra obtained under shock loading were fit with multiple Gaussian functions. The ambient spectrum was reproduced quite well with five fitting peaks. Even though the two modes at 3067 and 3076 cm^{-1} were not well-resolved, two peaks were needed in the fit. Three fitting peaks were used for the spectra at 3.0 and 3.5 GPa. At 4.5 and 5.5 GPa, a total of seven and eight fitting peaks were used, respectively. Figure 4 presents the results of peak fitting applied to the spectrum of the [111] orientation shocked to 5.5 GPa. These results are discussed in the next section.

The Raman spectra of shocked RDX [111] show a marked similarity to the Raman spectra of RDX under static pressure. From this finding, we infer that the RDX crystal undergoes a shock-induced transition to the γ phase above ~4 GPa. To our knowledge, this is the first real-time observation of a shock-induced phase transition in RDX. The exact pressure of the phase transition under shock loading was not determined but appears to occur between 3.5 and 4.5 GPa. This range agrees well with static pressure results that show the phase transition to occur between 3.8 and 4.0 GPa.[20,21,23] Some details regarding the α and γ phases, obtained from static pressure studies, are summarized below.

The α phase of RDX is orthorhombic with the *Pbca* space group.[22] Transition to the γ phase is reversible in the DAC and accompanied by a 1.6% reduction in volume. The crystal structure appears to remain orthorhombic.[23,40−42] The molecular point group symmetry of RDX in the α phase is C_s, with two of the NO_2 groups in the axial position and the third in the equatorial position; this is termed the axial−axial−equatorial, or AAE, conformation.[22] A structure for the γ phase has recently been published,[42] but there is some uncertainty regarding the molecular conformation in this phase.[43] We believe that the observed spectral changes in the CH stretching modes accompanying this phase transition are due to factor group, or Davydov, splitting caused by an abrupt increase in intermolecular interactions.[23] The exact nature of these interactions cannot be determined solely from our results, but a conformational change alone is not sufficient to produce the observed splitting. Further investigation will be required to better understand these structural changes. We have, however, shown that the $\alpha-\gamma$ phase transition can also be induced by shock wave loading to stresses above ~4 GPa.

B. Orientation Dependence. After discussing the observation of the phase transition under shock loading, we now examine the effect of crystal orientation on the Raman spectra. First, we consider the results obtained at stresses below ~4 GPa under static pressure and shock compression. A comparison of ambient spectra for the three RDX orientations is presented in Figure 5a. Relative intensities of the Raman modes differ among the orientations, but the positions are very similar. As indicated earlier, intensity differences are due to the relative orientation of the probe laser beam and the crystal axes.

A comparison of the three orientations at 3.0 GPa peak stress under shock loading is shown in Figure 5b. As at ambient pressure, there are differences in the relative intensities of the modes, but there is good agreement in the positions. These spectra were also fit by the procedure used for the [111] orientation. A comparison between the results from this fitting procedure and a more complete data set from the static pressure experiments[23] is shown in Figure 6. For static pressures to 3.5 GPa, the frequencies of the Raman modes increase with stress. Within experimental error, the shifting observed under shock loading at 3.0 GPa for all three orientations agrees with that measured under static pressure conditions. Error bars for the Raman frequencies observed in the shock experiments are based on the resolution of the detection system and uncertainty in the peak fitting analysis. The data at 3.5 GPa also fall on the same curves as the static pressure results. Thus, we conclude that there is no measurable orientation dependence in shock compression-induced Raman shifts up to 3.5 GPa.

At ~3.8 GPa static pressure, several Raman modes are clearly observed to split (see Figure 6). The mode initially at 2949 cm^{-1} splits into three modes. The two modes at 3067 and 3076 cm^{-1} collectively split into three modes. The 3003 cm^{-1} mode shifts to lower frequency at 3.8 GPa and splits at ~5 GPa. The 2906 cm^{-1} mode was not observed under shock; it is a weak combination mode[37] and is not included in this figure. The splitting of the Raman modes under static pressure conditions serves as a clear marker of the phase transition.[20,23]

Figure 5c shows a comparison of the spectra for each orientation from the experiments at 5.5 GPa peak stress. Although there is an overall agreement in the spectra for the three orientations, there are some differences, likely due to the orientation-dependent intensities of the modes and the broadening due to shock compression. The two peaks, around 3000 cm^{-1}, in the [210] data in Figure 5c are similar to the static results at 5.5 GPa in Figure 3b, but were not clearly resolved for the [100] and [111] orientations. The central peak in the spectrum for the [100] orientation saturated the detection system, giving it the odd, truncated shape.

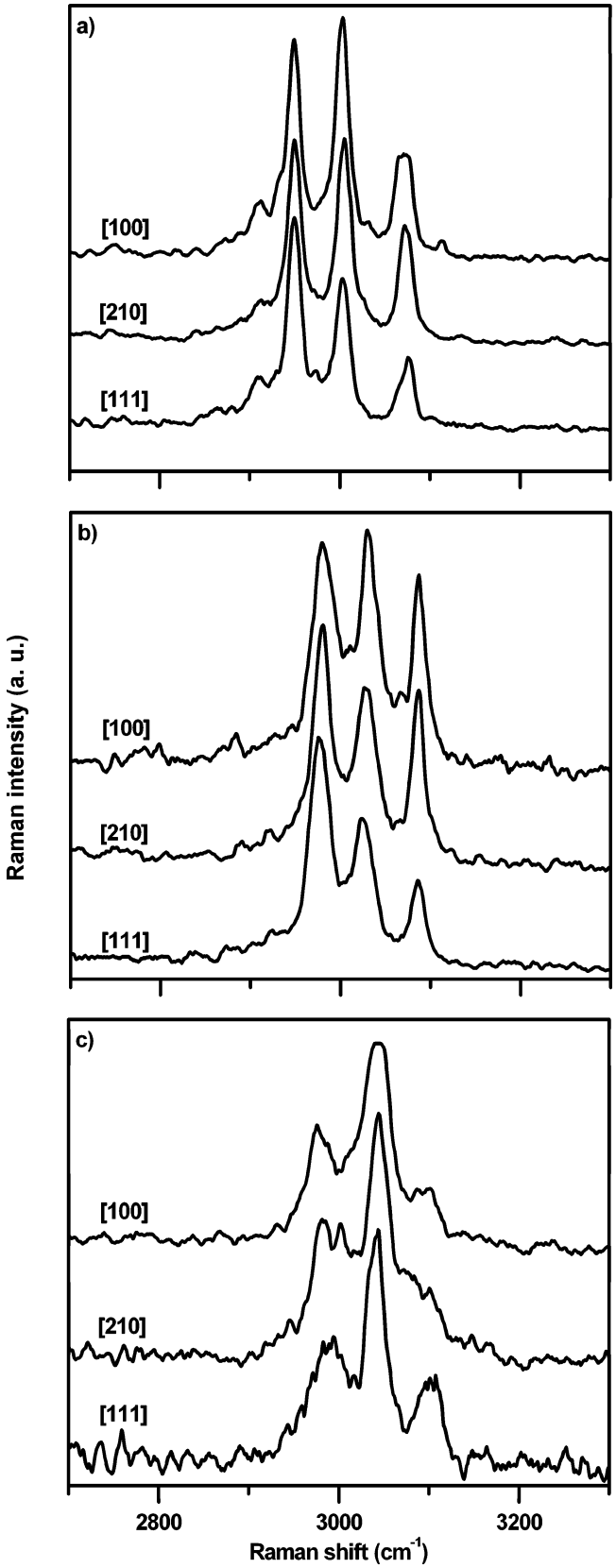

Figure 5. Comparison of Raman spectra for the three orientations of RDX at (a) ambient pressure, (b) 3.0 GPa, and (c) 5.5 GPa. Relative intensities differ among the orientations, but peak positions agree. Note that the Raman signal from the 5.5 GPa experiment for the [100] orientation saturated the detection system, truncating the central peak.

All the spectra in Figure 5c were fit by eight peaks, and the results of that analysis are also shown in Figure 6. Within the error bars, Figure 6 indicates good agreement of the peak

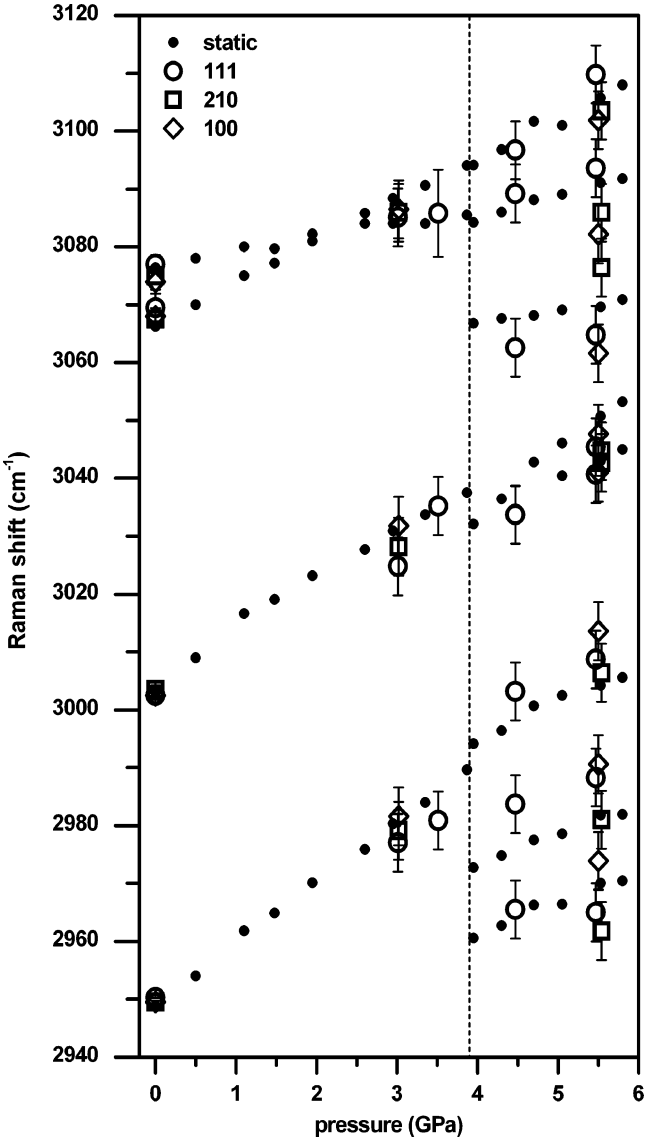

Figure 6. Summary plot of the frequencies of Raman modes vs pressure from shock and static compression experiments. The dashed line at 3.9 GPa indicates the boundary between the α and γ phases.

positions for the three orientations of RDX under shock loading and hydrostatic compression between 3.8 and 5.5 GPa. As already stated, this agreement between the static and shock results strongly indicates that the phase transition occurs under shock loading. In addition, these results indicate that the occurrence of the $\alpha-\gamma$ phase transition does not depend on crystal orientation.

At first glance, the lack of measurable anisotropy or orientation dependence in the Raman spectra seems a bit surprising due to the following reasons. First, it has been shown that the compressibility of RDX is different for the three crystallographic directions.[40] Second, shocks along different orientations should activate different numbers of the known slip systems. Recent wave profile measurements at 2.5 GPa show measurable differences for the orientations used in our experiments,[10] but it is unclear how these observations relate to the molecular response at stresses greater than 2.5 GPa. Phenomena such as dislocation slip involve interactions at the lattice level and are therefore highly directional, but they apparently do not play a significant role at the molecular level. Particle velocity profiles at stresses comparable to our experiments are needed to

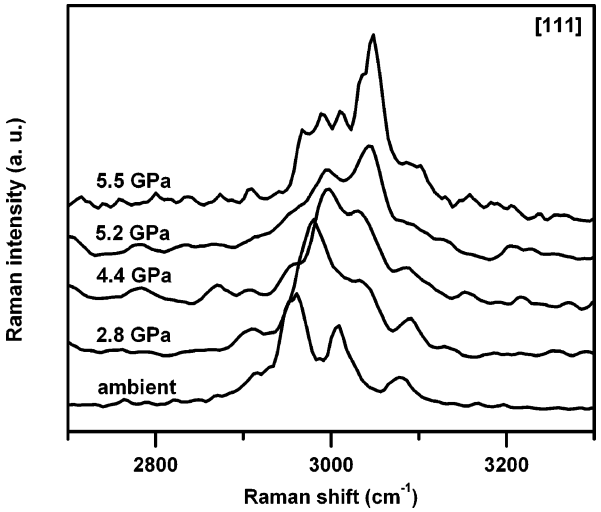

Figure 7. Time-resolved spectra taken during stepwise loading of the [111] orientation of RDX at 5.5 GPa peak stress. Spectra at ambient pressure and 5.5 GPa were averaged over 280 ns. The other three spectra were averaged over 50 ns and smoothed by five-point averaging. The spectrum at 4.4 GPa exhibits relative intensities similar to ambient pressure and 2.8 GPa. The spectrum at 5.2 GPa more closely resembles the spectrum at 5.5 GPa.

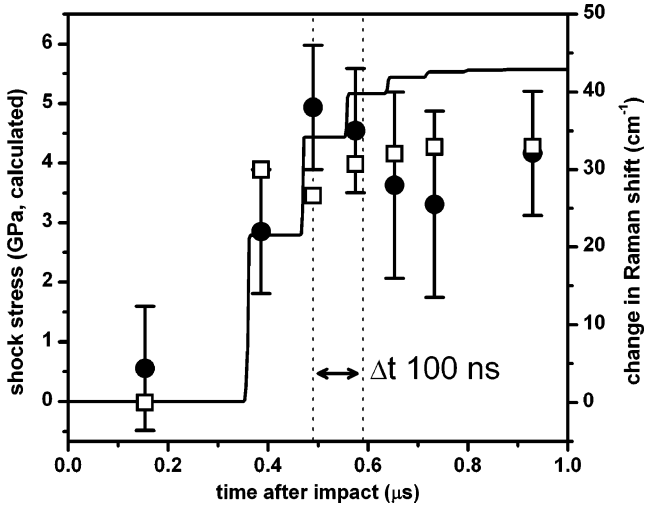

Figure 8. Comparison between projected and observed changes in peak position of the Raman mode initially at 2949 cm^{-1}. The solid line (left axis) is the calculated stress history at the midpoint of the RDX crystal. Open squares (right axis) indicate projected shifts based on static pressure data at the calculated stress. Closed circles (right axis) indicate observed shifts from the time-resolved measurement on [111]-oriented RDX.

understand the lack of anisotropy seen in our Raman data. These results for RDX are also different from what was observed for PETN, where crystal orientation had a noticeable effect on the shifting of the CH stretch modes.[6] Thus, the molecular level response of the two materials appears to be different and indicates the need for further examination of the factors governing anisotropy in shocked energetic crystals.

C. Dynamics of Phase Transition Under Shock Loading. Figure 7 shows selected spectra from the time-resolved Raman data for [111]-oriented RDX at 5.5 GPa peak stress. The stresses were calculated for the stepwise loading of RDX, between two Z-cut quartz windows, using a wave propagation code and a material model of RDX.[34,35] Stress increases with time. The ambient and 5.5 GPa spectra were binned over 280 ns of the streak camera record. These bins were chosen to cover times when the sample was in a state of uniform stress. The other three spectra were binned over 50 ns and smoothed by five-point adjacent averaging; the binning time was shorter because of the finite time between steps in the loading history. These bins were chosen such that the majority of the sample was at the same stress, even though the wave was reverberating through the RDX crystal.

In contrast to the results in Figure 2, the spectra at 2.8 and 4.4 GPa in Figure 7 are quite similar. Recall that these spectra in Figure 7 do not correspond to steady-state conditions, whereas the spectra in Figure 2 were taken at peak stresses. The Raman spectrum of RDX at 4.4 GPa in Figure 7 resembles the α phase spectrum. However, at a later time and higher stress, the spectrum more closely resembles that of the γ phase.

Comparing the time-dependent spectral shifts under shock loading with the static pressure shifts can provide insight into the phase transition dynamics. From the calculated stress history, we can project a time-dependent change in Raman shift for a particular mode by assuming that (i) the Raman shift is identical to that observed under hydrostatic compression and (ii) there is no time dependence in this shift. Below 3.8 GPa, we use the mode initially at 2949 cm^{-1}, and above 3.8 GPa, the new mode at 2973 cm^{-1}. The shifts of these modes are then compared to the shift of the lower frequency band in the spectra measured under shock compression.

In Figure 8, the solid line (left axis) shows the calculated stress history computed at the midpoint of the RDX sample under stepwise shock loading.[34,35] The shock wave enters the front of the RDX crystal 300 ns after impact. The open squares (right axis) indicate the projected Raman shift changes at particular times using the assumptions indicated above. There is a decrease in the projected shift between 390 and 490 ns (corresponding stresses are 3.5 and 4.5 GPa, respectively) due to the phase transition. As the stress increases above 4.5 GPa, the projected frequency shift increases gradually until reaching the value for 5.5 GPa.

The observed frequency shifts (right axis) are shown as closed circles. Unlike the projected shifts, the observed shift under shock compression continues to increase to higher frequency up to 490 ns (4.5 GPa). The observed spectra show that the decrease in the shift occurs at least 100 ns after the sample reached a stress state above 3.8 GPa. It is difficult to set an exact value for this delay time because not the entire sample is at the same state as the wave reverberates in the crystal. There is also some uncertainty in the calculated shock stress due to the material model used in the calculations. Additionally, the spectral resolution of the time-resolved system was not as high as the other spectroscopy systems used in this study. Despite these uncertainties, there is a clear difference between the projected and observed Raman shifts around the time that the stress state exceeds 4 GPa. At 900 ns, when the high resolution measurements were taken in the final state, the spectra obtained under static compression and shock loading are similar; the crystal had reached a steady state, and the structural transition was complete.

Thus, our results show that the phase transition does not occur immediately with a stress increase above 4.0 GPa, and the structural transformation displays time-dependence. A more detailed investigation of the kinetics would require several additional experiments and has not been pursued at this time. The important conclusion is that the phase transition requires finite time, on the order of 100 ns, to occur for the stress history

indicated in Figure 8. The incubation time likely depends on the load path; stronger shocks may cause the transition to occur more rapidly. Likewise, if the peak stress is not maintained sufficiently long, the phase transition will likely not occur.

D. Implications for Shock Initiation. Although the experiments in this study were performed well below the initiation threshold, these results are relevant to understanding the shock initiation of RDX. We have shown that the $\alpha-\gamma$ phase transition occurs under shock wave loading. Changes in intermolecular interactions may lead to conditions that are more favorable for the onset of chemical reactions.[44] Thus, the occurrence of the phase transition may be a prerequisite to initiation and should be included in detailed models of RDX decomposition.

Another example of how structural changes affect the onset of decomposition is the energetic material octahydro-1,3,5,7-tetranitro-*s*-tetrazocine (HMX). It has been shown that different polymorphs of HMX have different impact sensitivity,[45] and the polymorphs can be changed by material processing to achieve the desired performance for a particular application. In other words, HMX can be made to perform differently by properly modifying the material structure at ambient conditions.

Our results also indicate that the RDX response to shock compression differs from the PETN response. Unlike the RDX results, the Raman spectra of shocked PETN clearly showed different pressure-dependent shifts for different orientations and a discontinuity in the shifts of the CH stretch modes between 4 and 5 GPa.[6] The changes in the PETN Raman spectra were linked to a lowering of the molecular symmetry from S_4 to C_2.[3] However, the molecular symmetry of RDX is low at ambient conditions (C_s) and the molecules occupy sites of C_1 symmetry.[22] Thus, any change in the molecular conformation may not be observable by Raman spectroscopy. The changes we have observed are indicative of a structural change associated with the phase transition; changes in the molecular conformation are not required.

It remains to be seen whether RDX exhibits anisotropy for shock initiation, as was observed for PETN. Given that the phase transition occurs prior to initiation, it is possible that anisotropy in initiation will not be observed. As the material undergoes the phase transition, it may lose memory of its prior state and orientation. To fully understand the chemical decomposition of RDX under shock loading, the phase transition should be taken into account. The decomposition likely starts from the γ phase, which has intermolecular interactions that are different from those of the α phase.[23,42] Attempts to simulate the shock-induced decomposition of RDX in the solid phase have not explicitly considered the γ phase structure.[46] We are currently investigating the mechanisms governing shock-induced chemical decomposition and the effect of crystal orientation on the decomposition.

IV. Concluding Remarks

Raman measurements were obtained at stresses both below and above the $\alpha-\gamma$ phase transition (observed at 3.8 GPa in static pressure studies) in shocked RDX single crystals oriented along the [111], [210], and [100] directions. Both high-resolution and time-resolved Raman spectroscopy measurements were utilized. Spectral features consistent with static pressure measurements were observed under shock loading, suggesting that the $\alpha-\gamma$ phase transition takes place under shock compression. No significant orientation effects were observed in the molecular response of RDX to shock compression up to 5.5 GPa. The phase transition occurred after an incubation time of at least 100 ns when RDX was shocked to a peak stress of 5.5 GPa.

Even though all experiments were performed below the initiation threshold, this study represents an important first step in understanding the shock-induced chemical decomposition of RDX. We have shown that the transition to the γ phase takes place at stresses below 5.5 GPa. This structural change involves an increase in intermolecular interactions[23] that likely serve to precondition the material for the onset of chemical decomposition at higher stresses. Thus, theoretical studies of shocked RDX for chemical decomposition need to incorporate the γ-phase structure. Further investigation is required to determine the specific mechanisms governing this decomposition and to determine if RDX exhibits anisotropic behavior in its initiation response. Differences between the RDX and PETN shock response illustrate the importance of investigating multiple HE crystals to determine whether the observed properties are material-specific or apply to HE crystals more generally. Experimental studies at higher stresses to examine initiation are underway.

Acknowledgment. The authors thank Dr. Daniel E. Hooks of the Los Alamos National Laboratory for providing the RDX crystals. Dr. Naoki Hemmi is thanked for advice and assistance in setting up the high-resolution Raman system. Dr. J. Michael Winey is thanked for the stress wave calculations and comments on this manuscript. Kurt Zimmerman and Kent Perkins are thanked for their assistance in performing the shock experiments. This work was supported by ONR MURI Grant N00014-01-1-0802 and DOE Grant DEFG0397SF21388.

References and Notes

(1) Gruzdkov, Y. A.; Gupta, Y. M. *J. Phys. Chem. A* **2000**, *104*, 11169.
(2) Dreger, Z. A.; Gruzdkov, Y. A.; Gupta, Y. M.; Dick, J. J. *J. Phys. Chem. B* **2002**, *106*, 247.
(3) Gruzdkov, Y. A.; Dreger, Z. A.; Gupta, Y. M. *J. Phys. Chem. A* **2004**, *108*, 6216.
(4) Dick, J. J. *J. Appl. Phys.* **1997**, *81*, 601.
(5) Yoo, C. S.; Holmes, N. C.; Souers, P. C.; Wu, C. J.; Ree, F. H.; Dick, J. J. *J. Appl. Phys.* **2000**, *88*, 70.
(6) Hemmi, N.; Dreger, Z. A.; Gruzdkov, Y. A.; Winey, J. M.; Gupta, Y. M. *J. Phys. Chem. B* **2006**, *110*, 20948.
(7) Haussuhl, S. *Z. Kristallogr.* **2001**, *216*, 339.
(8) Schwarz, R. B.; Hooks, D. E.; Dick, J. J.; Archuleta, J. I.; Martinez, A. R. *J. Appl. Phys.* **2005**, *98*, 056106/1.
(9) Haycraft, J. J.; Stevens, L. L.; Eckhardt, C. J. *J. Chem. Phys.* **2006**, *124*, 024712/1.
(10) Hooks, D. E.; Ramos, K. J.; Martinez, A. R. *J. Appl. Phys.* **2006**, *100*, 024908/1.
(11) Sandusky, H. W.; Beard, B. C.; Glancy, B. C.; Elban, W. L.; Armstrong, R. W. *Mat. Res. Soc. Symp. Proc.* **1993**, *296*, 93.
(12) Owens, F. J.; Sharma, J. *J. Appl. Phys.* **1980**, *51*, 1494.
(13) Forbes, J. W.; Tasker, D. G.; Granholm, R. H.; Gustavson, P. K. In *Shock Compression of Condensed Matter − 1989*; Schmidt, S. C., Johnson, J. N., Davison, L. W., Eds.; AIP: New York 1990; p 709.
(14) Delpuech, A.; Cherville, J.; Michaud, C. In *Proc. Seventh Symp. (Int.) on Detonation*; Short, J. M., Ed.; Naval Surface Weapon Center, 1981; p 65.
(15) Delpuech, A.; Mentil, A.; Pouligny, B. In *Shock Waves Condens. Matter − 1985*; Gupta, Y. M., Ed.; Plenum: New York 1986; p 877.
(16) McCrone, W. C. *Anal. Chem.* **1950**, *22*, 954.
(17) Karpowicz, R. J.; Brill, T. B. *J. Phys. Chem.* **1983**, *87*, 2109.
(18) Karpowicz, R. J.; Sergio, S. T.; Brill, T. B. *Ind. Eng. Chem. Prod. Res. Dev.* **1983**, *22*, 363.
(19) Karpowicz, R. J.; Brill, T. B. *J. Phys. Chem.* **1984**, *88*, 348.
(20) Baer, B. J.; Oxley, J.; Nicol, M. *High Pressure Res.* **1990**, *2*, 99.
(21) Miller, P. J.; Block, S.; Piermarini, G. J. *Combust. Flame* **1991**, *83*, 174.
(22) Choi, C. S.; Prince, E. *Acta Crystallogr.* **1972**, *B28*, 2857.
(23) Dreger, Z. A.; Gupta, Y. M. *J. Phys. Chem. B* **2007**, *111*, 3893.
(24) Maharrey, S.; Behrens, R.; Jr. *J. Phys. Chem. A* **2005**, *109*, 11236.
(25) Boyd, S.; Gravelle, M.; Politzer, P. *J. Chem. Phys.* **2006**, *124*, 104508/1.
(26) Strachan, A.; Kober, E. M.; van Duin, A. C. T.; Oxgaard, J.; Goddard, W. A., III. *J. Chem. Phys.* **2005**, *122*, 054502/1.
(27) Botcher, T. R.; Wight, C. A. *J. Phys. Chem.* **1994**, *98*, 5441.
(28) Yoo, C. S.; Gupta, Y. M.; Horn, P. D. *Chem. Phys. Lett.* **1989**, *159*, 178.
(29) Gustavsen, R. L.; Gupta, Y. M. *J. Appl. Phys.* **1994**, *75*, 2837.

(30) Pangilinan, G. I.; Gupta, Y. M. *J. Phys. Chem.* **1994**, *98*, 4522.
(31) Gallagher, H. G.; Halfpenny, P. J.; Miller, J. C.; Sherwood, J. N. *Philos. Trans. R. Soc. London, Ser. A* **1992**, *339*, 293.
(32) Johnson, J. N.; Jones, O. E.; Michaels, T. E. *J. Appl. Phys.* **1970**, *41*, 2330.
(33) Winey, J. M. Personal communication.
(34) Gupta, Y. M. COPS code; Stanford Research Institute, Menlo Park, CA, 1976; unpublished.
(35) Winey, J. M. unpublished results.
(36) Rey-Lafon, M.; Trinquecoste, C.; Cavagnat, R.; Forel, M. T. *J. Chim. Phys. Phys.-Chim. Biol.* **1971**, *68*, 1533.
(37) Haycraft, J. J.; Stevens, L. L.; Eckhardt, C. J. *J. Appl. Phys.* **2006**, *100*, 053508/1.
(38) Rice, B. M.; Chabalowski, C. F. *J. Phys. Chem. A* **1997**, *101*, 8720.
(39) Park, T.-R.; Dreger, Z. A.; Gupta, Y. M. *J. Phys. Chem. B* **2004**, *108*, 3174.
(40) Olinger, B.; Roof, B.; Cady, H. In *Symposium on High Dynamic Pressures*; Commissariat a l'Energie Atomique: Saclay, France, 1978; p 3.
(41) Yoo, C.-S.; Cynn, H.; Howard, W. M.; Holmes, N. In *Eleventh Int. Detonation Symp.*; Office of Naval Research: Arlington, VA, 1998; p 951.
(42) Goto, N.; Fujihisa, H.; Yamawaki, H.; Wakabayashi, K.; Nakayama, Y.; Yoshida, M.; Koshi, M. *J. Phys. Chem. B* **2006**, *110*, 23655.
(43) Goto, N.; Yamawaki, H.; Wakabayashi, K.; Nakayama, Y.; Yoshida, M.; Koshi, M. *Sci. Technol. Energ. Mater.* **2005**, *66*, 291.
(44) Cohen, M. D.; Schmidt, G. M. J. *J. Chem. Soc., Abstracts* **1964**, 1996.
(45) Herrmann, M.; Engel, W.; Eisenreich, N. *Propellants, Explos., Pyrotech.* **1992**, *17*, 190.
(46) Strachan, A.; van Duin, A. C. T.; Chakraborty, D.; Dasgupta, S.; Goddard, W. A., III. *Phys. Rev. Lett.* **2003**, *91*, 098301/1.